Available online at www.sciencedirect.com
SCIENCE DIRECT
Journal of Power Sources 152 (2005) 122–130
JOURNAL OF POWER SOURCES
www.elsevier.com/locate/jpowsour

Mathematical modeling of a passive-feed DMFC with heat transfer effect

R. Chen, T.S. Zhao *

Department of Mechanical Engineering, The Hong Kong University of Science and Technology, Clear Water Bay, Kowloon, Hong Kong SAR, China

Received 12 January 2005; accepted 10 February 2005
Available online 31 May 2005

Abstract

A passive liquid-feed direct methanol fuel cell (DMFC) with neither external liquid pumps nor gas blowers is modeled mathematically. A one-dimensional model is developed by considering inherently coupled heat and mass transport, along with the electrochemical reactions occurring in passive DMFCs. The analytical solutions predicting the performance of this type of fuel cell operating with different methanol concentrations are obtained. It is shown that the performance of passive DMFCs increases with methanol concentration. It is further revealed that the improved performance with higher methanol concentrations is due primarily to the increased operating temperature resulted from the exothermic reaction between permeated methanol and oxygen on the cathode.

Keywords: Fuel cell; Passive DMFC; Heat and mass transfer; Thermal effect; Thermal management

1. Introduction

The direct methanol fuel cell (DMFC) is an electrochemical device that directly converts chemical energy into electrical energy. Because of its high efficiency, high energy density, low emission, and simple structure, the DMFC has been projected to be a prime candidate for powering portable devices [1]. In terms of fuel and oxidant delivery schemes, DMFCs can be classified either as active-feed DMFCs or as passive-feed DMFCs.

In active-feed DMFCs, methanol solution is usually delivered by a liquid pump, while oxidant (oxygen or air) is supplied by a gas blower/fan. To improve cell performance, most previous studies on active-feed DMFCs have been focused on the following aspects: improving the electroactivity of methanol oxidation on the anode by exploring more active electrocatalysts [2–4]; optimizing cathode electrode structures to avoid severe flooding [5]; investigating the effect of methanol crossover [6–11]; reducing the substantial methanol crossover by modifying existing polymer membranes [12] or searching for alternatives [13]; flow field designs and CO_2 management [14–19].

In contrast, the concept of passive DMFCs is that a DMFC can operate stand-alone, eliminating the external means of liquid transport and air movement. Therefore, the fuel cell system becomes much simpler and more compact. This concept provides a unique feature for the miniaturization of fuel cells. For this reason, passive DMFCs have recently received much attention. Kim et al. [20] fabricated and tested a single cell and monopolar DMFC stack operating under passive and air-breathing conditions. Liu et al. [21] studied sintered stainless steel fiber felt as the gas diffusion layer in an air-breathing DMFC. Shimizu and Momma [22] reported their activities regarding the research and development of DMFCs that operated passively at room temperature. Chen and Yang [23] investigated the effect of operating conditions on the power density of an air-breathing DMFC.

As compared with their active counterparts, passive-feed DMFCs have much lower power density (about 20 mW cm^{-2}) because of two major problems. One is the inability to handle the excess water evolved on the cathode

* Corresponding author. Tel.: +852 2358 8647; fax: +852 2358 1543.
E-mail address: metzhao@ust.hk (T.S. Zhao).

0378-7753/$ – see front matter © 2005 Elsevier B.V. All rights reserved.
doi:10.1016/j.jpowsour.2005.02.088

and crossed from the anode. The other is that conventional designs lose too much heat from the fuel cell to the ambient air, resulting in rather low cell operating temperatures (less than 30 °C). Therefore, the ambient conditions under which passive DMFCs operate require added attention to be given to thermal and water management.

Because several interrelated processes occur simultaneously, the development of a mathematical model is critical to the design and the optimization of passive-feed DMFCs. In particular, understanding thermal effects, which are inseparable from the management of water in the cell, is necessary to optimize the performance of these fuel cells. A number of studies [24–34] have been reported simulating PEM fuel cells and DMFCs, but most of them were isothermal models, except for a few papers that took into account thermal effects for simulating solid oxide fuel cells [35–37]. Nordlund and Lindbergh [30] proposed an isothermal agglomerate model based on the reaction mechanism for the electrochemical oxidation of methanol to study the influence of the porous structure on the direct methanol fuel cells. Wang and Wang [31] used two-phase multi-component model to simulate a DMFC. The anode and cathode electrochemical reactions, diffusion and convection of both gas and liquid phases in the backing layers and flow channels, mixed potential effect due to methanol crossover and the effect of methanol feed concentration were explored. Murgia et al. [32] developed a one-dimensional, two-phase, multi-component steady-state model based on the phenomenological transport equations. In their model, the influences of the methanol concentration, the pressure gradient in the catalyst layer, flooding in the cathode gas diffusion layer, and methanol crossover on the cell performance were investigated.

In this paper, we present a theoretical model that incorporates the effects of coupled heat and mass transfer and electrochemical kinetics in a passive-feed DMFC. We demonstrate that this simplified model is capable of shedding light on the mechanisms leading to a better performance when this type of fuel cells operate with higher methanol concentrations under ambient conditions.

2. Model development

Consider a passive-feed DMFC shown in Fig. 1, which consists of a fuel tank, an anode current collector (ACC), an anode gas diffusion layer (AGDL), an anode catalyst layer (ACL), a membrane, a cathode catalyst layer (CCL), a cathode gas diffusion layer (CGDL), and a cathode current collector (CCC). On the anode, diluted methanol solution is introduced to the reaction zone without any external means of liquid transport. From the ACC through the AGDL and finally to the ACL, methanol solution is transported primarily by diffusion. After the electrochemical reaction of methanol oxidation, CO_2 produced at the ACL moves counter-currently toward the fuel tank via the AGDL and ACC. At sufficiently high current densities, CO_2 emits in

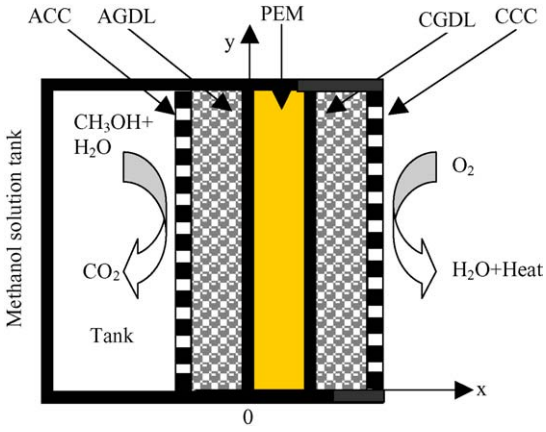

Fig. 1. Schematic of a passive liquid-feed DMFC.

the form of gas bubbles from the surface of the ACC. For the vertically orientated DMFC shown in Fig. 1, in the fuel tank, due to buoyancy, CO_2 moves upwards adjacent to the surface of the ACC, while the liquid methanol solution away from the surface of the ACC moves downwards. As such, the diffusion of methanol solution from the fuel tank to the ACC is virtually enhanced by natural convection. On the cathode of this passive-feed DMFC, oxygen is taken passively from the ambient air without any means of air movement. Almost all the heat generated by the fuel cell is lost from the vertical CCC to the ambient, leading to natural heat convection at the surface of the CCC. The mass transport of oxygen and water on the cathode is enhanced by natural convection.

It is clear from the above description that the operation of the passive-feed DMFC considered in this work actually involves rather complex transport processes of heat and mass, which are linked to the electrochemical reactions of methanol oxidation on the anode and oxygen reduction on the cathode. To make the complicated process tractable, we treat it as a one-dimensional problem, with the x-axis origin set at the ACL, as illustrated in Fig. 1. We also introduce the following simplifications and assumptions:

(1) The fuel cell is assumed to operate under steady-state conditions.
(2) Compared with the heat generated by electrochemical reaction and overpotential, Joule heat caused by the current flow through each component is ignored.
(3) The fuel tank, ACC, and AGDL are well insulated from the ambient. No heat is lost from these components to the ambient. Thus, the temperature at each of these components is the same as that at ACL.
(4) Considering that ACL and CCL are much thinner than AGDL, CGDL and the membrane, they are treated as an interface and the temperature and concentration distributions are uniform.
(5) The transport of heat and mass through the gas diffusion layers is assumed to be a diffusion-predominated process and the convection effect due to bulk flow is ignored.

(6) On the cathode, the heat and mass are transferred between the CCC and the ambient by natural convection.
(7) On the anode, the mass transfer of methanol from the bulk solution to the ACC is assumed to be driven by natural convection. For a sufficiently large fuel tank, the methanol concentration in the tank during the fuel cell discharging is assumed to be constant.
(8) Methanol crossover through the membrane is assumed to be due to the combined effect of the concentration gradient between the anode and cathode and the electro-osmosis force.
(9) Since the reaction rate of methanol on the cathode is rather fast, the methanol concentration in the CCL is assumed to be depleted.

2.1. Mass transport

The transport process of methanol from the fuel tank to the ACC is described by:

$$N_{\mathrm{m}} = h_{\mathrm{m}}(C_{\mathrm{m,tank}} - C^{0}_{\mathrm{m,acc}}), \tag{1}$$

where N_{m} represents the methanol flux, h_{m} the mass transfer coefficient at the ACC surface, and $C^{0}_{\mathrm{m,acc}}$ and $C_{\mathrm{m,tank}}$ are the methanol concentrations at the ACC surface and in the tank, respectively.

In the ACC and AGDL, since no electrochemical reaction occurs, the methanol flux remains the same and is related to the concentration gradient by Fick's law as:

$$N_{\mathrm{m}} = -D^{\mathrm{eff}}_{\mathrm{m,acc}} \frac{\mathrm{d}C_{\mathrm{m,acc}}}{\mathrm{d}x}, \tag{2}$$

and

$$N_{\mathrm{m}} = -D^{\mathrm{eff}}_{\mathrm{m,agdl}} \frac{\mathrm{d}C_{\mathrm{m,agdl}}}{\mathrm{d}x}, \tag{3}$$

where $D^{\mathrm{eff}}_{\mathrm{m,acc}}$ and $D^{\mathrm{eff}}_{\mathrm{m,agdl}}$ represent the effective diffusion coefficients of methanol in the ACC and AGDL, respectively. Combining Eqs. (1)–(3) yields:

$$N_{\mathrm{m}} = \alpha_1(C_{\mathrm{m,tank}} - C_{\mathrm{m,acl}}), \tag{4}$$

where $\alpha_1 = \left(\frac{l_{\mathrm{agdl}}}{D^{\mathrm{eff}}_{\mathrm{m,agdl}}} + \frac{l_{\mathrm{acc}}}{D^{\mathrm{eff}}_{\mathrm{m,acc}}} + \frac{1}{h_{\mathrm{m}}} \right)^{-1}$.

The methanol flux, N_{m}, is related to the proton current density, i_{a}, and the permeation flux of methanol through the membrane, N_{cross}, by:

$$N_{\mathrm{m}} = \frac{1}{6F} i_{\mathrm{a}} + N_{\mathrm{cross}}, \tag{5}$$

where F is the Faraday's constant (96,485 C mol^{-1}). The current density, i_{a}, can be determined from the Tafel equation:

$$i_{\mathrm{a}} = i^{\mathrm{m}}_{\mathrm{ref}} \frac{C_{\mathrm{m,acl}}}{C^{\mathrm{m}}_{\mathrm{ref}}} \exp\left(\frac{\alpha_{\mathrm{a}} F}{RT_{\mathrm{acl}}} \eta_{\mathrm{a}} \right), \tag{6}$$

where $i^{\mathrm{m}}_{\mathrm{ref}}$ and $C^{\mathrm{m}}_{\mathrm{ref}}$ represent, respectively, the reference exchange current density on the anode and the reference concentration of methanol, and $C_{\mathrm{m,acl}}$ is the methanol concentration in the ACL. The permeation flux of methanol through the membrane, N_{cross}, can be determined from:

$$N_{\mathrm{cross}} = -D^{\mathrm{eff}}_{\mathrm{m,mem}} \frac{\mathrm{d}C_{\mathrm{m,mem}}}{\mathrm{d}x} + n^{\mathrm{m}}_{\mathrm{d}} \frac{i}{F}, \tag{7}$$

where $D^{\mathrm{eff}}_{\mathrm{m,mem}}$ is the effective diffusion coefficient of methanol in the membrane and $n^{\mathrm{m}}_{\mathrm{d}}$ is the electro-osmotic drag coefficient of methanol.

On the cathode, oxygen extracted from the air reacts with the electron and proton to produce water. Additionally, part of oxygen is consumed due to methanol crossover to form an internal current and a mixed potential. Therefore, the oxygen flux from the CGDL to the CCL can be determined from:

$$N_{\mathrm{O_2}} = \frac{1}{4F} i_{\mathrm{c}} + \frac{3}{2} N_{\mathrm{cross}}. \tag{8}$$

To account for the effect of methanol crossover on the cathode overpotential, we assume that the methanol from the anode completely reacts electrochemically on the cathode. Based on this assumption, the internal current, i_{p}, due to the methanol oxidation on the cathode can be obtained based on the permeation flux of methanol [31]:

$$i_{\mathrm{p}} = 6FN_{\mathrm{cross}}. \tag{9}$$

It follows from Eqs. (6) and (9) that the cathode overpotential taking account of the mixed potential can be determined from:

$$i_{\mathrm{c}} + i_{\mathrm{p}} = i^{\mathrm{O_2}}_{\mathrm{ref}} \frac{C_{\mathrm{O_2,ccl}}}{C^{\mathrm{O_2}}_{\mathrm{ref}}} \exp\left(\frac{\alpha_{\mathrm{c}} F}{RT_{\mathrm{ccl}}} \eta_{\mathrm{c}} \right), \tag{10}$$

where $i^{\mathrm{O_2}}_{\mathrm{ref}}$ and $C^{\mathrm{O_2}}_{\mathrm{ref}}$ represent, respectively, the reference exchange current density on the cathode and the reference concentration of oxygen, and $C_{\mathrm{O_2,ccl}}$ is the oxygen concentration in the CCL.

In the CGDL and CCC, the oxygen flux remains the same and is related to the concentration gradient by:

$$N_{\mathrm{O_2}} = -D^{\mathrm{eff}}_{\mathrm{O_2,cgdl}} \frac{\mathrm{d}C_{\mathrm{O_2,cgdl}}}{\mathrm{d}x}, \tag{11}$$

and

$$N_{\mathrm{O_2}} = -D^{\mathrm{eff}}_{\mathrm{O_2,ccc}} \frac{\mathrm{d}C_{\mathrm{O_2,ccc}}}{\mathrm{d}x}, \tag{12}$$

where $D^{\mathrm{eff}}_{\mathrm{O_2,cgdl}}$ and $D^{\mathrm{eff}}_{\mathrm{O_2,ccc}}$ represent, respectively, the effective diffusion coefficients of oxygen in the CGDL and in the CCC.

The oxygen transport from the ambient air to the CCC is due to natural convection and can be described by:

$$N_{\mathrm{O_2}} = h_{\mathrm{O_2}}(C_{\mathrm{O_2,amb}} - C^{0}_{\mathrm{O_2,ccc}}), \tag{13}$$

where $h_{\mathrm{O_2}}$ is the mass transfer coefficient of oxygen on the cathode, $C^{0}_{\mathrm{O_2,ccc}}$ and $C_{\mathrm{O_2,amb}}$ are the oxygen concentrations

at the surface of the CCC and in the bulk air, respectively. Combining Eqs. (11)–(13) gives the oxygen flux as:

$$N_{O_2} = \alpha_2(C_{O_2,amb} - C_{O_2,ccl}), \quad (14)$$

where $\alpha_2 = \left(\frac{1}{h_{O_2}} + \frac{l_{cgdl}}{D^{eff}_{O_2,cgdl}} + \frac{l_{ccc}}{D^{eff}_{O_2,ccc}}\right)^{-1}$.

2.2. Heat transport

On the anode, heat, generated by the electrochemical reaction in the ACL, is given by:

$$q_{acl} = i\left(\eta_a - \frac{\Delta H_a - \Delta G_a}{nF}\right), \quad (15)$$

where the first term represents the heat due to the activation and mass transfer overpotentials on the anode, the second term represents the entropy change of the anodic electrochemical reaction, with ΔH_a denoting the anodic reaction enthalpy and ΔG_a the Gibbs free energy. Eq. (15) can be rewritten as [38]:

$$q_{acl} = i\eta_a - \beta_1 - \beta_2(T_{acl} - 298), \quad (16)$$

where $\beta_1 = \frac{i}{6F}(\Delta H^0_a - \Delta G^0_a)$ and $\beta_2 = \frac{i}{6F}(C_{CO_2} - C_m - C_{H_2O})$.

Neglecting Joule heat in the membrane, we can relate the heat flux, q_{acl}, to the temperature gradient across the membrane as:

$$q_{acl} = -\lambda_{mem}\frac{dT}{dx}, \quad (17)$$

where λ_{mem} is the effective thermal conductivity of the membrane.

The heat generation on the CCL, q_{ccl}, can be determined from:

$$q_{ccl} = (i + i_p)\eta_c - i\frac{\Delta H_c - \Delta G_c}{nF} - h_v N_{H_2O}, \quad (18)$$

where the first term represents the heat due to activation and mass transfer overpotentials and mixed potential caused by methanol crossover on the cathode; the second term accounts for the entropic loss, with ΔH_c denoting the cathodic reaction enthalpy and ΔG_c is the Gibbs free energy; the third term reflects the heat due to the evaporation of liquid water at the CCL, with h_v denoting the latent heat of water and N_{H_2O} is the flux of water evaporation. Eq. (18) can be rewritten as:

$$q_{ccl} = (i + i_p)\eta_c - \beta_3 - \beta_4(T_{ccl} - 298) - h_v N_{H_2O}, \quad (19)$$

where $\beta_3 = \frac{i}{2F}(\Delta H^0_c - \Delta G^0_c)$ and $\beta_4 = \frac{i}{2F}\left(C_{H_2O} - \frac{1}{2}C_{O_2}\right)$.

We assume that the air at the CCC is in a saturated state based on the following justifications: in addition to the water continuously generated on the cathode, the permeation rate of water from the anode to cathode is relatively high in DMFCs, even under the open circuit voltage (OCV) condition [34]. In particular, in passive DMFCs, more water may be accumulated on the cathode due to the limited removal rate of water with no external means of air movement. Then, the flux of water evaporation can also be determined by natural convection:

$$N_{H_2O} = h_{H_2O}(C^{sat}_{H_2O,ccc} - C_{H_2O,amb}), \quad (20)$$

where h_{H_2O} denotes the mass transfer coefficient of water vapor on the cathode, $C^{sat}_{H_2O,ccc}$ and $C_{H_2O,amb}$ are the water vapor concentrations at the surface of the CCC and in the bulk air, respectively. The water vapor concentration can be determined from P_{H_2O}/RT, and the saturated pressure of moist air is determined from [27]:

$$P_{sat} = 10^{(-2.1794 + 0.02953\times T - 9.1837\times 10^{-5}\times T^2 + 1.4454\times 10^{-7}\times T^3)}. \quad (21)$$

The total heat generation q_{tot} is given by:

$$q_{tot} = q_{acl} + q_{ccl}, \quad (22)$$

which is related to the temperature gradient in the CGDL and the CCC, respectively, to

$$q_{tot} = -\lambda_{cgdl}\frac{dT}{dx}, \quad (23)$$

and

$$q_{tot} = -\lambda_{ccc}\frac{dT}{dx}, \quad (24)$$

where λ_{cgdl} and λ_{ccc} represent the effective thermal conductivities of in the CDGL and in the CCC. Finally, the heat transfer from the CCC to the ambient air can be described using the Newton's cooling law as:

$$q_{tot} = h_t(T^0_{ccc} - T_{amb}), \quad (25)$$

where h_t is the heat transfer coefficient due to natural convection, T^0_{ccc} and T_{amb} are the temperatures at the surface of the CCC and the ambient air. Combining Eqs. (23)–(25), we obtain:

$$q_{tot} = \alpha_3(T_{ccl} - T_{amb}), \quad (26)$$

where $\alpha_3 = \left(\frac{1}{h_t} + \frac{l_{cgdl}}{\lambda_{cgdl}} + \frac{l_{ccc}}{\lambda_{ccc}}\right)^{-1}$.

The heat transfer coefficient at the surface of the CCC can be determined from [39]:

$$Nu = \frac{hL}{\lambda} = 0.68 + \frac{0.67Ra_L^{1/4}}{[1 + (0.492/Pr)^{9/16}]^{4/9}}, \quad (27)$$

where Ra_L is the Rayleigh number ($Ra_L = GrPr$), Pr the Prandtl number, and Gr is the Grashof number $\left(Gr = \frac{\beta g(T_W - T_0)L^3}{\nu^2}\right)$. Based on the analogy principle between heat and mass transfer, the mass transfer coefficient can also be determined from Eq. (27) with Nu replaced by Sherwood number, $Sh = \frac{h_{mass}L}{D}$, and Pr replaced by Lewis number, $Le = Sh/Nu$ (for gas $Le = 1$ [40]). On the anode, the

natural convection is caused by bubble behavior. The mass transfer coefficient at the ACC is determined by assuming that $Sh/Nu = 2.0$.

2.3. Cell performance

With the methanol/oxygen concentration at the catalyst layers and the temperature distributions, and the anodic and cathodic overpotentials obtained from the equations presented above, we can assess the cell performance based on:

$$V_{\text{cell}} = E_{\text{cell}} - \eta_{\text{a}} - \eta_{\text{c}} - iR_{\text{cell}}, \tag{28}$$

where E_{cell} is the thermodynamic equilibrium potential of the fuel cell and is a function of temperature and pressure, and R_{cell} is the internal resistance of the fuel cell. The thermodynamic equilibrium potentials of the fuel cell can be calculated by:

$$E_{\text{cell}} = E^0_{\text{cell}} + \Delta T\left(\frac{\partial E}{\partial T}\right), \tag{29}$$

where E^0_{cell} is the open circuit voltage at $T = 298\,\text{K}$ and $(\partial E/\partial T)$ represents the rate of change of electromotive force.

3. Analytical solutions

We now obtain analytical solutions from the equations presented in the preceding section. Combining Eqs. (4), (5), and (7) yields the methanol concentration at the ACL:

$$C_{\text{m,acl}} = \frac{\alpha_1 C_{\text{m,tank}} - \frac{i}{6F}}{\frac{D^{\text{eff}}_{\text{m,mem}}}{l_{\text{mem}}} + 1.8\times10^{-5} n_{\text{H}_2\text{O}}\frac{i}{F} + \alpha_1}. \tag{30}$$

With the aide of Eq. (30), the oxygen concentration at the CCL can be determined by using Eqs. (8) and (14) to give:

$$C_{\text{O}_2,\text{ccl}} = \frac{1}{\alpha_2}\left(\alpha_2 C_{\text{O}_2,\text{amb}} - \frac{i}{4F} - \frac{3}{2}\left(D^{\text{eff}}_{\text{m,mem}}\frac{C_{\text{m,acl}}}{l_{\text{mem}}} + 1.8\times10^{-5} n_{\text{H}_2\text{O}}\frac{i}{F}\right)\right). \tag{31}$$

Table 1
Physical properties

Parameter/symbol (unit)	Value	Refs.
Liquid methanol enthalpy of formation/H_{m} (J mol^{-1})	-238.66×10^3	
Liquid water enthalpy of formation/ΔH_{w} (J mol^{-1})	-285.83×10^3	
Carbon dioxide enthalpy of formation/ΔH_{CO_2} (J mol^{-1})	-393.51×10^3	
Liquid methanol Gibbs free energy/ΔG_{m} (J mol^{-1})	-166.27×10^3	
Liquid water Gibbs free energy/ΔG_{w} (J mol^{-1})	-237.08×10^3	
Carbon dioxide Gibbs free energy/ΔG_{CO_2} (J mol^{-1})	-394×10^3	
Liquid methanol specific heat capacity/c_{m} ($\text{J mol}^{-1}\,\text{K}^{-1}$)	80.96	
Liquid water specific heat capacity/c_{w} ($\text{J mol}^{-1}\,\text{K}^{-1}$)	75.24	
Carbon dioxide specific heat capacity/c_{CO_2} ($\text{J mol}^{-1}\,\text{K}^{-1}$)	36.9	
Oxygen specific heat capacity/c_{O_2} ($\text{J mol}^{-1}\,\text{K}^{-1}$)	39.44	
Evaporation heat of water/h_{v} (J mol^{-1})	44.86×10^3	
Pressure of air in cathode/P_0 (Pa)	1×10^5	
Oxygen concentration in the ambient air/$C_{\text{O}_2,\text{amb}}$ (mol m^{-3})	$0.21\times P/RT$	
Thickness of ACC and CCC/l_{acc} (m)	0.001	Assumed
Thickness of AGDL and CGDL/l_{agdl} (m)	0.0003	[41]
Electro-osmotic drag coefficient of water/$n_{\text{H}_2\text{O}}$	$2.9\exp(1029/(1/333-1/T))$	[42]
Electro-osmotic drag coefficient of methnaol/n^{m}_{d}	$x_{\text{m}}\times n_{\text{H}_2\text{O}}$	[31]
Conductivity of membrane/σ_{m} (S m^{-1})	$7.3\exp(1268(1/298-1/T))$	[43]
Correction factor of diffusion coefficient/ε	0.6	Assumed
Thermal conductivity of membrane/λ_{mem} ($\text{W m}^{-1}\,\text{K}^{-1}$)	0.21	[33]
Thermal conductivity of CGDL/λ_{cgdl} ($\text{W m}^{-1}\,\text{K}^{-1}$)	1.6	[44]
Thermal conductivity of CCC/λ_{ccc} ($\text{W m}^{-1}\,\text{K}^{-1}$)	16	
Diffusion coefficient of methanol in membrane/$D^{\text{eff}}_{\text{m,mem}}$ ($\text{m}^2\,\text{s}^{-1}$)	$4.9\times10^{-10}\exp(2436(1/333-1/T))$	[43]
Diffusion coefficient of methanol in ACC/$D^{\text{eff}}_{\text{m,acc}}$ ($\text{m}^2\,\text{s}^{-1}$)	2.8×10^{-9}	[34]
Diffusion coefficient of methanol in AGDL/$D^{\text{eff}}_{\text{m,agdl}}$ ($\text{m}^2\,\text{s}^{-1}$)	$2.8\times10^{-9}\varepsilon$	
Diffusion coefficient of oxygen in CCC and air/$D^{\text{efff}}_{\text{O}_2,\text{ccc}}$ ($\text{m}^2\,\text{s}^{-1}$)	0.25×10^{-4}	
Diffusion coefficient of oxygen in CGDL/$D^{\text{eff}}_{\text{O}_2,\text{cgdl}}$ ($\text{m}^2\,\text{s}^{-1}$)	$0.25\times10^{-4}\varepsilon$	
Diffusion coefficient of water vapor in air/$D^{\text{eff}}_{\text{H}_2\text{O,air}}$ ($\text{m}^2\,\text{s}^{-1}$)	6×10^{-4}	Assumed
Transfer coefficient of anode/α_{a}	0.35	Assumed
Transfer coefficient of cathode/α_{c}	0.8	Assumed
Reference concentration of methanol/$C^{\text{m}}_{\text{ref}}$ (mol m^{-3})	4×10^3	Assumed
Reference concentration of oxygen/$C^{\text{O}_2}_{\text{ref}}$ (mol/m^3)	$0.21\times P_0/RT$	
Reference exchange current density on anode/$i^{\text{m}}_{\text{ref}}$ (A m^{-2})	$94.25\exp(35{,}570/R(1/353-1/T))$	[31]
Reference exchange current density on cathode/$i^{\text{O}_2}_{\text{ref}}$ (A m^{-2})	$0.04222\exp(73{,}200/R(1/353-1/T))$	[31]
Rate of change of electromotive force/∂E/∂T (V K^{-1})	-1.4×10^{-4}	[34]

Utilizing the calculated methanol and oxygen concentrations at the catalyst layer, the temperatures at catalyst layer are obtained from Eqs. (16), (17), (19), (22), and (26). The temperatures in the ACL and the CCL is given, respectively, as:

$$T_{\mathrm{acl}} = \left[\frac{i\eta_{\mathrm{a}} - \beta_1 + 298\beta_2 + \eta_{\mathrm{c}}(i+i_{\mathrm{p}}) - \beta_3 + 298\beta_4 + \frac{l_{\mathrm{mem}}}{\lambda_{\mathrm{mem}}}(i\eta_{\mathrm{a}}\beta_4 - \beta_1\beta_4 + 298\beta_2\beta_4 - \alpha_3\beta_1 + 298\beta_2\alpha_3 + i\eta_{\mathrm{a}}\alpha_3) + \alpha_3 T_{\mathrm{amb}} - h_{\mathrm{v}} N_{\mathrm{H_2O}}}{\alpha_3 + \beta_2 + \beta_4 + \frac{l_{\mathrm{mem}}}{\lambda_{\mathrm{mem}}}(\beta_2\alpha_3 + \beta_2\beta_4)} \right]. \quad (32)$$

and

$$T_{\mathrm{ccl}} = T_{\mathrm{acl}} - \frac{l_{\mathrm{mem}}}{\lambda_{\mathrm{mem}}}(i\eta_{\mathrm{a}} - \beta_1 - T_{\mathrm{acl}}\beta_2 + 298\beta_2). \quad (33)$$

It should be mentioned that the heat and mass transfer coefficients are determined based on the iteration procedure by presuming a wall temperature at the CCC surface. Iteration will not cease until a right wall temperature and right heat, and mass transfer coefficients, obtained from Eq. (27), are determined such that the total heat generated is balanced by the heat loss from the cathode to the ambient. The results to be presented in the next section were obtained based on the parameters listed in Table 1.

4. Results and discussion

Fig. 2 shows the temperature distribution in the cell when it is filled with 2 M methanol solution and operates at different current densities. The four data points represent, respectively, the temperatures at the ACL, the CCL, the CGDL/CCC interface, and the outer surface of the CCC. It is seen from Fig. 2a that at a lower current density the temperature on the anode is lower than that on the cathode. This is because the heat generation rate by the anodic overpotential at low current densities is less than the endothermic heat demanded by the electrochemical reaction of methanol oxidation. As a result, some heat has to be taken from the cathode. With an increase in current density, the heat generation rate by the anodic overpotential increases. Therefore, as indicated in Fig. 2b, the temperature on the anode becomes higher than that on the cathode. With a further increase in current density, the temperature difference between the anode and cathode increases, as evident by comparing Fig. 2b and c.

Fig. 3 shows the polarization curves when the fuel cell operates with 1 M, 2 M, 3 M, and 4 M methanol solutions, respectively. It can be seen from this figure that with an increase in methanol concentration, the cell performance upgrades progressively. A higher methanol concentration results in a higher methanol permeation rate from the anode side to the cathode side. On the cathode side, methanol reacts with the oxygen electrochemically to form a mixed potential. Hence, a higher methanol concentration leads to a higher mixed potential, thereby causing a higher heat generation rate. As a result, a higher concentration results in a higher operating temperature. This is evident from Fig. 4, which shows the variation in the temperature at the ACL with current density for different methanol concentrations. The increased operating temperature improves the electrochemical reactions of both methanol oxidation and oxygen reduction, producing a higher voltage for a given current density. Therefore, it can be concluded that the improved cell performance with a higher methanol concentration is primarily attributed to

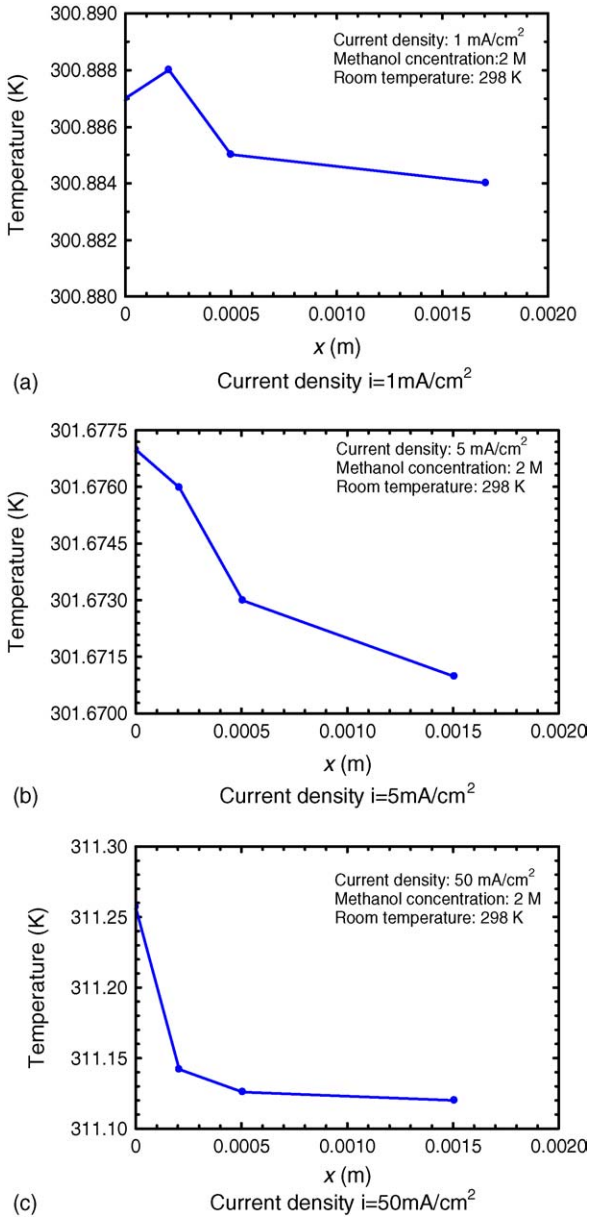

Fig. 2. Temperature distribution in the cell at different current densities: (a) current density, $i = 1\,\mathrm{mA\,cm^{-2}}$, (b) $i = 5\,\mathrm{mA\,cm^{-2}}$, and (c) $i = 50\,\mathrm{mA\,cm^{-2}}$.

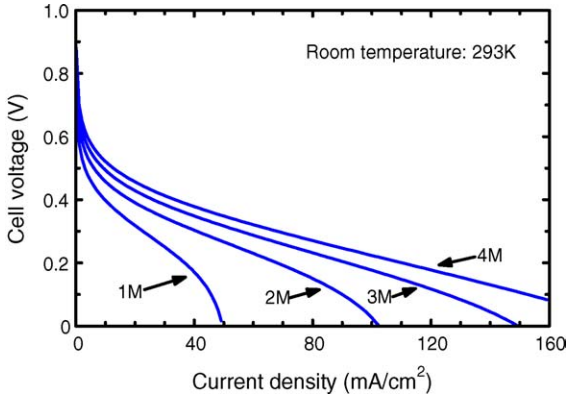

Fig. 3. Polarization curves of the passive DMFC operating with different methanol concentrations.

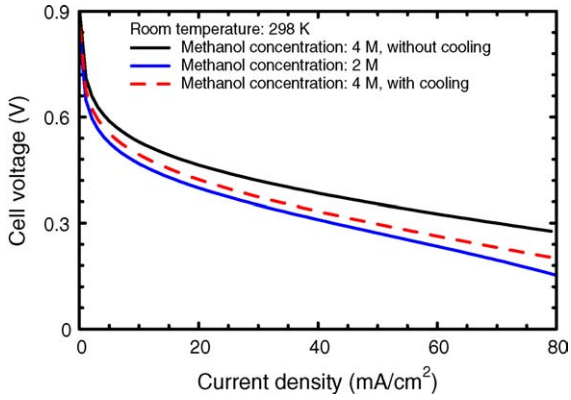

Fig. 5. Polarization curves for the 4 M methanol operation with and without the operating temperature lowered to the value of the 2 M methanol operation under the OCV condition.

the increased operating temperature caused by the exothermic reaction between permeated methanol and oxygen on the cathode. It is also noted from Fig. 4 that for each methanol concentration, the temperature at the ACL increases with current density. This is because the heat generation rate due to activation and mass transfer activation increase with an increase in current density.

In order to further verify that the improved cell performance with higher methanol concentrations is due to the increased operating temperature caused by higher methanol permeation rates, we now let the passive DMFC still operate with 4 M methanol, but remove the excess heat generated from the system by cooling down the cell to a lower temperature. Fig. 5 presents the performance, represented by the dashed curve, of the fuel cell operating with 4 M methanol and at an operating temperature controlled to be the same as that when the cell operates with 2 M methanol under the open circuit voltage condition. For comparison, the polarization curves with 2 M and 4 M without cooling are also shown in Fig. 5. It can be seen from this figure that feeding 4 M methanol solution with a lowed operating temperature results in significantly lower performance than feeding the same concentration methanol without cooling does. Although the performance with 4 M methanol at the lowered operating temperature becomes much lower than that without the control of the operating temperature, it is still a bit higher than that with 2 M methanol. This may be due to the higher mass transfer rate with a higher methanol concentration. The results presented in Fig. 5 indicate that the excess heat generated by the exothermic reaction of the permeated methanol on the cathode is removed from the cell, the cell performance declines and becomes almost the same as that with 2 M methanol. The comparison in cell performance among the three operating conditions confirms that the improved performance of a passive DMFC running with higher methanol concentrations is attributed primarily to the higher operating temperature caused by the exothermic reaction between the permeated methanol and oxygen on the cathode.

The effect of room temperature on the cell performance with different methanol concentrations is shown in Fig. 6. It is clear from this figure that the cell performance increases with room temperature. The lower heat loss rate to the ambient with a higher room temperature creates a higher operating temperature, causing the electrochemical kinetics of

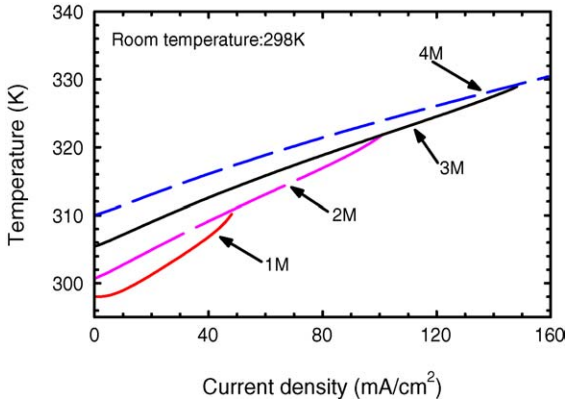

Fig. 4. Variations in the operating temperature (at the anode catalyst layer) with current density for different methanol concentrations.

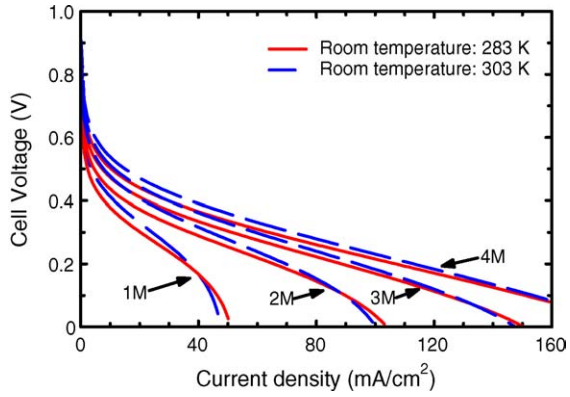

Fig. 6. Polarization curves for different methanol concentrations and at different room temperatures.

both methanol oxidation and oxygen reduction to be improved. The results presented in Fig. 6 suggest that the performance of a passive DMFC is sensitive to a change in ambient conditions.

5. Concluding remarks

A one-dimensional thermal model for passive DMFCs is developed. Inherently coupled heat and mass transport, along with the electrochemical reactions, are considered. The analytical solutions of methanol and oxygen concentration, and temperature distributions through the cell components are obtained. The performance of the fuel cell fed with different methanol concentrations (1–4 M) is predicted. It has been shown that at low current densities, the temperature on the anode is lower than that on the cathode. With an increase in current density, the temperature on the anode becomes higher than that on the cathode. A higher current density leads to a higher temperature difference between the anode and cathode. Furthermore, with this model it has been revealed that passive DMFCs operating with a higher methanol concentration yield a better performance. The improved performance with higher methanol concentrations has been found to be due primarily to the higher operating temperature caused by the exothermic reaction between the permeated methanol and oxygen on the cathode. The results presented in this work suggest that thermal management in passive DMFCs is critical for improving the performance of this type of fuel cells.

Acknowledgement

The work described in this paper was fully supported by a grant from the Research Grants Council of the Hong Kong Special Administrative Region, China (Project No. HKUST6197/03E).

References

[1] C.K. Dyer, Fuel cells for portable applications, J. Power Sources 106 (2002) 31–34.
[2] J. Prabhuram, T.S. Zhao, C.W. Wong, et al., Preparation and structural/electrochemical characterization of Pt/C nanocatalyst for polymer electrolyte fuel cells, J. Power Sources 134 (2004) 1–6.
[3] D. Cao, S.H. Bergens, Pt–Ru_{adatom} nanoparticles as anode catalysts for direct methanol fuel cells, J. Power Sources 134 (2004) 170–180.
[4] J.W. Guo, T.S. Zhao, J. Prabhuram, C.W. Wong, Preparation and physical/electrochemical properties of Pt/C nanocatalyst stabilized by citric acid for polymer electrolyte fuel cells, Electrochim. Acta 50 (2005) 1973–1983.
[5] S.C. Thomas, X. Ren, S. Gottesfeld, P. Zelenay, Direct methanol fuel cells: progress in cell performance and cathode research, Electrochim. Acta 47 (2002) 3741–3748.
[6] Z. Qi, A. Kaufman, Open circuit voltage and methanol crossover in DMFCs, J. Power Sources 110 (2004) 177–185.
[7] Q. Ye, T.S. Zhao, H. Yang, J. Prabhuram, Electrochemical reactions in a DMFC under open circuit conditions, Electrochem. Solid State Lett. 8 (2005) A52–A54.
[8] N. Munichandraiah, K. McGrath, G.K.S. Prakash, et al., A potentiometric method of monitoring methanol crossover through polymer electrolyte membranes of direct methanol fuel cells, J. Power Sources 117 (2003) 98–101.
[9] J. Prabhuram, T.S. Zhao, H. Yang, Methanol adsorbates on the DMFC cathode and their effect on the cell performance, J. Electroanal. Chem. 578 (2005) 105–112.
[10] A. Heinzel, V.M. Barragán, A review of the state-of-the-art of the methanol crossover in direct methanol fuel cells, J. Power Sources 84 (1999) 70–74.
[11] Q. Ye, T.S. Zhao, Electrolytic hydrogen evolution in DMFCs induced by oxygen interruptions and its effect on cell performance, Electrochem. Solid State Lett. 8 (2005) A211–A214.
[12] T. Hejze, B.R. Gollas, R.K. Sauerbrey, et al., Preparation of Pd-coated polymer electrolyte membranes and their application in direct methanol fuel cells, J. Power Sources 140 (2005) 21–27.
[13] B. Xing, O. Savadogo, Hydrogenroxygen polymer electrolyte membrane fuel cells PEMFCs based on alkaline-doped polybenzimidazole PBI, Electrochem. Commun. 2 (2000) 697–702.
[14] H. Yang, T.S. Zhao, Q. Ye, In situ visualization study of CO_2 gas bubble behavior in DMFC anode flow fields, J. Power Sources 139 (2005) 79–90.
[15] H. Yang, T.S. Zhao, Q. Ye, Addition of non-reacting gases to the anode flow field of DMFCs leading to improved performance, Electrochem. Commun. 6 (2004) 1098–1103.
[16] A.S. Aricò, P. Cretì, V. Baglio, E. Modica, V. Antonucci, Influence of flow field design on the performance of a direct methanol fuel cell, J. Power Sources 91 (2000) 202–209.
[17] C.W. Wong, T.S. Zhao, Q. Ye, J.G. Liu, Transient capillary blocking in the flow field of a micro DMFC and its effect on cell performance, J. Electrochim. Soc. 157 (7) (2005).
[18] K. Tüber, A. Oedegaard, M. Hermann, C. Hebling, Investigation of fractal flow-fields in portable proton exchange membrane and direct methanol fuel cells, J. Power Sources 131 (2004) 175–181.
[19] H. Yang, T.S. Zhao, Q. Ye, Pressure drop behavior in the anode flow field of liquid feed DMFCs, J. Power Sources 142 (2005) 117–124.
[20] D. Kim, E.A. Cho, S.A. Hong, I.H. Oh, H.Y. Ha, Recent progress in passive direct methanol fuel cells at KIST, J. Power Sources 130 (2004) 172–177.
[21] J.G. Liu, G.Q. Sun, F.L. Zhao, et al., Study of sintered stainless steel fiber felt as gas diffusion backing in air-breathing DMFC, J. Power Sources 133 (2004) 175–180.
[22] T. Shimizu, T. Momma, et al., Design and fabrication of pumpless small direct methanol fuel cells for portable applications, J. Power Sources 137 (2004) 277–283.
[23] C.Y. Chen, P. Yang, Performance of an air-breathing direct methanol fuel cell, J. Power Sources 123 (2003) 37–42.
[24] J.J. Baschuk, X.G. Li, Modelling of polymer electrolyte membrane fuel cells with variable degrees of water flooding, J. Power Sources 86 (2003) 181–196.
[25] T. Berning, D.M. Lu, N. Djilali, Three-dimensional computational analysis of transport phenomena in a PEM fuel cell, J. Power Sources 106 (2002) 284–294.
[26] D.M. Bernardi, Water-balance calculation for solid-polymer-electrolyte fuel cells, J. Electrochem. Soc. 137 (1990) 2244–2250.
[27] T.E. Springer, T.A. Zawodzinski, S. Gottesfeld, Polymer electrolyte fuel cell model, J. Electrochem. Soc. 138 (1991) 2334–2342.
[28] T.F. Fuller, J. Newman, Water and thermal management in solid-polymer-electrolyte fuel cells, J. Electrochem. Soc. 140 (1993) 1218–1225.
[29] W.S. He, J.S. Yi, T.V. Nguyen, Two-phase flow model of the cathode of PEM fuel cells using interdigitated flow fields, AIChE J. 46 (2000) 2053–2064.
[30] J. Nordlund, G. Lindbergh, A model for the porous direct methanol fuel cells anode, J. Electrochem. Soc. 149 (9) (2002) A1107–A1113.
[31] Z.H. Wang, C.Y. Wang, Mathematical modeling of liquid-feed direct methanol fuel cells, J. Electrochem. Soc. 150 (4) (2003) A508–A519.

[32] G. Murgia, L. Pisani, A.K. Shukla, K. Scott, A numerical model of a liquid-feed solid polymer electrolyte DMFC and its experimental validation, J. Electrochem. Soc. 150 (9) (2003) A1231–A1245.
[33] P. Argyropoulos, K. Scott, W.M. Taama, One-dimensional thermal model for direct methanol fuel cell stacks. Part I. Model development, J. Power Sources 79 (1999) 169–183.
[34] K. Scott, P. Argyropoulos, K. Sundmacher, A model for the liquid feed direct methanol fuel cell, J. Electroanal. Chem. 477 (1999) 97–110.
[35] P.W. Li, L. Schaefer, M.K. Chyu, A numerical model coupling the heat and gas species' transport processes in a tubular SOFC, J. Heat Transfer Trans. ASME 126 (2004) 219–229.
[36] P.W. Li, K. Suzuki, Numerical modeling and performance study of a tubular SOFC, J. Electrochem. Soc. 151 (4) (2004) A548–A557.
[37] J.L. Yuan, M. Rokni, B. Sunden, Three-dimensional computational analysis of gas and heat transport phenomena in ducts relevant for anode-supported solid oxide fuel cells, Int. J. Heat Mass Transfer 46 (5) (2003) 809–821.
[38] J.M. Smith, Chemical Engineering Kinetics, third international ed., McGraw-Hill, Singapore, 1981.
[39] P.W. Li, T. Zhang, Q.M. Wang, et al., The performance of PEM fuel cells fed with oxygen through the free-convection mode, J. Power Sources 114 (2003) 63–69.
[40] A. Mongruel, M. Cloitre, C. Allain, Scaling of boundary-layer flows driven by double-diffusive convection, Int. J. Heat Mass Transfer 39 (1996) 3899–3910.
[41] K. Scott, W.M. Taama, S. Kramer, P. Argyropoulos, K. Sundmacher, Limiting current behaviour of the direct methanol fuel cell, Electrochim. Acta 45 (1999) 945–957.
[42] H. Guo, C.F. Ma, 2D analytical model of a direct methanol fuel cell, Electrochem. Commun. 6 (2004) 306–312.
[43] K. Scott, W.M. Taama, J. Cruickshank, Performance and modelling of a direct methanol solid polymer electrolyte fuel cell, J. Power Sources 65 (1997) 159–171.
[44] A. Rowe, X.G. Li, Mathematical modeling of proton exchange membrane fuel cells, J. Power Sources 102 (2001) 82–96.